Ultramicroscopy 207 (2019) 112835

Contents lists available at ScienceDirect

Ultramicroscopy

journal homepage: www.elsevier.com/locate/ultramic

Electron spill-out effects in plasmon excitations by fast electrons

Alberto Rivacoba

Departamento de Física de Materiales, Facultad de Ciencias Químicas, UPV/EHU, Materials Physics Center (CSIC-UPV/EHU), MPC and and Donostia International Physics Center (DIPC), P. Manuel de Lardizabal 5 20018 San Sebastián, Spain

ARTICLE INFO

Keywords:
EELS Electron microscopy
Dispersion relation of Interface plasmons

ABSTRACT

A new non-retarded hydrodynamic approach to the interaction between a fast electron and a diffuse metal-vacuum interface is presented. The metal is characterized by the parameters of a dispersive bulk dielectric function which slowly fade at the interface. The response of the medium is described by the induced charge density, which is self-consistently calculated. This formalism is applied to the study of the energy loss spectrum (*EELS*) experienced by a fast electron passing by a metal-vacuum interface. In the case of a sharp interface analytical expressions for the loss probability, fully equivalent to that of the Specular Reflection Model *(SRM)*, are found. In an Al interface the effects of the electron density spill-out (modeled according to Lang-Kohn density) on both the longitudinal (*EELS*) and transverse components of the momentum transfer are studied. The influence of the interface profile on the surface plasmon dispersion in *EELS* is also discussed, showing that in agreement with previous theoretical and experimental works the dispersion of surface plasmon turns out to be much weaker than the one calculated in the *SRM*. A possible extension of the theory to study interfaces between transition metals and insulators is also discussed.

1. Introduction

Following Ritchie's seminal paper [1], the local dielectric formalism has been widely used to study the excitation of plasmons in bounded targets by fast electron-probes. In this approach the excitations of the target are given by the local dielectric function $\epsilon(\omega)$, which only depends on frequency ω. In the non-retarded limit the energy loss experienced by a probe interacting with a target is calculated from the induced potential, that in the case of sharp interfaces can be obtained by solving the Poisson equation with the customary boundary conditions at the surface. In the case of targets of simple geometry, such as planes, films, small particles or wires, the energy loss probability experienced by the probe admits simple analytical solutions (see for instance Ref.[2]). For targets of more complicated shapes the induced potential must be numerically computed by using the so called *Boundary Element Method* (*BEM*) [3]. The main advantage of the local formalism lies in the possibility of using experimental dielectric functions, a procedure which leads to good qualitative and quantitative agreement in *EELS* in *Scanning Transmission Electron Microscope (STEM)* for a wide range of media [4–7]. The local approach has been also applied to study the plasmon excitations in metallic interfaces with a smoothly varying electron density profile [8,9]. The dielectric approach has been also extended to the study of retardation effects in planes [10–13], cylinders [14,15], spheres [16], dimers [17,18], flakes [19], tapers [20] and in arbitrarily shaped interfaces [21].

Nevertheless, when the probe penetrates the target or travels very close to its surface the local response is not longer appropriate because it fails to describe the decreasing ability of the valence electrons to respond collectively to large wave vector components of the exciting field, a fact which leads to a logarithmic divergence in the induced potential at the probe position. This unphysical divergence is usually avoided by imposing a cutoff to the momentum contribution [22]. Besides, the local theory fails to reproduce the quadratic dispersion of the bulk plasmon energy experimentally found, $\omega_p(\mathbf{k}) = \omega_p + \alpha\mathbf{k}^2$, where $\mathbf{k}$ is the plasmon wave vector [23–25]. A proper treatment of this effect requires account to be taken of the $\mathbf{k}$ dependence of the medium response. The recent experiment carried out by Batson and coworkers [26], showing that the attractive or repulsive character of the transverse force experienced by a nanoparticle under the action of a STEM beam depends on the impact parameter, also implies that a proper description of the momentum carried by the interface excitations is needed to soundly study this problem.

The most extended way to implement the dispersion is to use a k dependent dielectric function $\epsilon(k, \omega)$, which describes the polarization created by a probe in an isotropic unbounded medium. The first dispersive response function of a homogeneous electron gas calculated by Lindhard [27] was modified by Mermin to account for the damping [28]. These dielectric functions describe the full range of excitation of

E-mail address: alberto.rivacoba@ehu.eus.

https://doi.org/10.1016/j.ultramic.2019.112835
Received 17 December 2018; Received in revised form 19 August 2019; Accepted 28 August 2019
Available online 29 August 2019

the electron gas, and are rather complicated. In the case of fast electron-probes only small k values give significant contribution to the plasmon excitation probability, so that simpler approximate expressions for $\epsilon(k, \omega)$ are generally used. The simplest approximation is the so called Hydrodynamic Dielectric Function (HDF) [29]:

$$\epsilon(k, \omega) = 1 - \frac{\omega_p^2}{\omega(\omega + i\gamma) - \beta^2 k^2}, \tag{1}$$

where ω_p is the frequency of the undispersed bulk plasmon, γ the damping constant, which represents the inverse of the plasmon lifetime, and β a constant, which accounts for the finite compressibility of the electron gas. For a homogeneous electron gas the electron density n determines the values of both parameters:

$$\begin{aligned} \omega_p^2 &= 4\pi n, \\ \beta^2 &= \frac{3}{5}[3\pi^2 n]^{\frac{2}{3}}. \end{aligned} \tag{2}$$

This dielectric function is valid in the range of plasmon excitations $k < \omega_p v_F^{-1}$, where v_F is the Fermi velocity of the medium, a limit which corresponds to the threshold of electron-hole excitations. In the range of collective excitations in a typical STEM experiments, where the beam energy is of the order of 100 keV, almost all the electrons are scattered with momentum transfer smaller than this limit, so that this dielectric function can be safely used.

Ritchie pointed out the difficulty of applying the nonocal dielectric formalism to metallic interfaces [1]. The fact that even in a sharp interface the induced charge density is not constrained to the surface or to the probe position [30] forces to restate the problem of the boundary conditions, which can not be simply written in terms of the continuity of the fields at the interface, as in the local approach. To overcome this problem in sharp planar metallic interfaces Ritchie and Marusak [31] and Wagner [32] proposed a method based on the Semiclassical Infinite Barrier, generally known as *Specular Reflection Model* (*SRM*), where one assumes that the electrons of the target are specularly reflected at the interface. In this approach all the surface effects are given by an induced charge density that spreads out inside the interface according to the bulk dielectric function $\epsilon(k, \omega)$. This model leads to a linear dispersion relation of the surface plasmon. In the case of fast electron-probes, this method allows calculation of the induced potential in a relatively simple way in terms of a new function $\tilde{\epsilon}(\mathbf{k}_\parallel, \omega)$, where $\mathbf{k}_\parallel$ stands for the components of the momentum parallel to the surface [33,34]. This model has been extended to deal with targets of different geometries: spheres [35,36], dimers [37], cylinders [38] and films [39].

The main drawback of the *SRM* is that it is not extendable to interfaces where the unperturbed charge density presents a smooth profile. In the case of metallic surfaces the spill-out of the electron density is of the order of few atomic units (a_0), so that short wave length fields are needed to probe it [40]. In optical experiments, where the large wave length of the probe makes the response insensitive to the shape of the density profile, the sharp interface model has been recently applied to study nonlocal effects in the optical response of nanoparticles [41–44]. Nevertheless the sharp surface approach is not longer justified when the interface is probed by fast charges, because the high momentum components of the evanescent field created by the probe can effectively probe the interface region. To account for nonlocal effects on the energy of the surface modes of diffuse interfaces the hydrodynamic model has been widely applied [45–49].

A theoretical approach to *EELS* in diffuse interfaces is also needed to thoroughly interpret plasmon mapping in interfaces between alloys or composite materials [50], where the loss peak energy at a given position is usually interpreted as an indicator of the *local* charge density at the spot. The local dielectric approach presented by Howie and coworkers showed that in broad interfaces corrections to the *local* peak energy are small [9]. The soundness of this approach is compromised by the fact that it just considers the interface plasmon shift associated to the spatial profile of the background density, without taking into account the effects derived from the nonlocality of the response of the medium.

The aim of this paper is to present a formalism able to be applied to the study of the polarization of spatially spread interfaces by a STEM probe. As a first step we study the effect of the electron spill-out on the energy loss spectra of fast electrons moving near metallic interfaces. We present an alternative non-retarded formulation of the dynamics of the electron gas, where a $\mathbf{k}$ dependent term accounting for the kinetic pressure of the electron gas is heuristically introduced into the plasma motion equation, in such a way that in two well known limiting cases (homogeneous medium and sharp planar interface) one recovers the results of the dielectric theory for the HDF (Eq. (1)). Then this formalism is applied to calculate the probability of exciting plasmons in an Al interface modeled according to the electron density profile calculated by Lang and Kohn [51]. The extension of this theory to more complex interfaces is discussed in the last section of this paper.

Atomic units are used in the theoretical developmment, while in the discussion of the results and in the plots the units nm, eV and $\AA^{-1}$ commonly used by experimentalist have been favored. The definition of some functions has been made clear by adding a tilde over them: so for instance, $\widetilde{\omega_p^2}(\mathbf{r})$ and $\widetilde{\omega_p^2}(\mathbf{k})$ stand respectively, for the function defined as the square of the *local* plasmon frequency at $\mathbf{r}$ and its Fourier transform, while ω_p is just the value of the bulk plasmon frequency in the homogeneous medium. Out of simplicity the induced charge density will be referred as just $\rho(\mathbf{k}, \omega)$, using the notation $\rho_0(\mathbf{k}, \omega)$ for the probe charge density.

Finally, in this work the following convention for the Fourier transform has been used:

$$f(\mathbf{k}, \omega) = \int d\mathbf{r}\, dt\, f(\mathbf{r}, t) e^{-i(\mathbf{kr} - \omega t)}. \tag{3}$$

2. The hydrodynamic model

Let us consider the excitation of an inhomogeneous electron gas where in the absence of external field the charge density is a function of the position $n(\mathbf{r})$. Under the effect of an external field $\mathbf{E}_0(\mathbf{r}, t)$, the displacement $\boldsymbol{\xi}(\mathbf{r}, t)$ of the charge in a given volume dV is given by:

$$dm \frac{\partial^2}{\partial t^2} \boldsymbol{\xi}(\mathbf{r}, t) = dq\, [\mathbf{E}_0(\mathbf{r}, t) - \nabla \int d\mathbf{r}' \frac{\rho(\mathbf{r}', t)}{|\mathbf{r} - \mathbf{r}'|}], \tag{4}$$

where dm and dq are respectively, the mass and charge contained in the volume dV and $\rho(\mathbf{r}, t)$ stands for the induced charge density. The integral in the right hand term accounts for the electric potential created by the induced charge. For the sake of simplicity, we have not introduced the damping term, which will be added later. In the ω space this equation can be recast as

$$\omega^2 \boldsymbol{\xi}(\mathbf{r}, \omega) = -\mathbf{E}_0(\mathbf{r}, \omega) + \nabla \int d\mathbf{r}' \frac{\rho(\mathbf{r}', \omega)}{|\mathbf{r} - \mathbf{r}'|}, \tag{5}$$

where we have made use of the fact that $dq/dm = 1$. The continuity equation, $\nabla \cdot \mathbf{J}(\mathbf{r}, \omega) = i\omega\rho(\mathbf{r}, \omega)$, provides a relation between the two fields $\rho(\mathbf{r}, \omega)$ and $\boldsymbol{\xi}(\mathbf{r}, \omega)$:

$$\rho(\mathbf{r}, \omega) = -\nabla \cdot [n(\mathbf{r}) \boldsymbol{\xi}(\mathbf{r}, \omega)], \tag{6}$$

which can be used to remove $\boldsymbol{\xi}(\mathbf{r}, \omega)$ from Eq. (5). After some simple algebra the following scalar equation is obtained:

$$\begin{aligned} &[\omega(\omega + \imath\gamma) - \widetilde{\omega_p^2}(\mathbf{r})]\rho(\mathbf{r}, \omega) + \frac{1}{4\pi} \nabla \widetilde{\omega_p^2}(\mathbf{r}) \cdot \nabla \int d\mathbf{r}' \frac{\rho(\mathbf{r}', \omega)}{|\mathbf{r}' - \mathbf{r}|}] \\ &\quad = \widetilde{\omega_p^2}(\mathbf{r}) \rho_0(\mathbf{r}, \omega) + \frac{1}{4\pi} \nabla \widetilde{\omega_p^2}(\mathbf{r}) \cdot \mathbf{E}_0(\mathbf{r}, \omega), \end{aligned} \tag{7}$$

where $\rho_0 = \frac{1}{4\pi} \nabla \cdot \mathbf{E}_0$ is the probe charge density and the function $\widetilde{\omega_p^2}(\mathbf{r}) = 4\pi n(\mathbf{r})$ stands for the frequency of the *local* plasmon at $\mathbf{r}$. Here a constant damping γ has been introduced in a straightforward way.

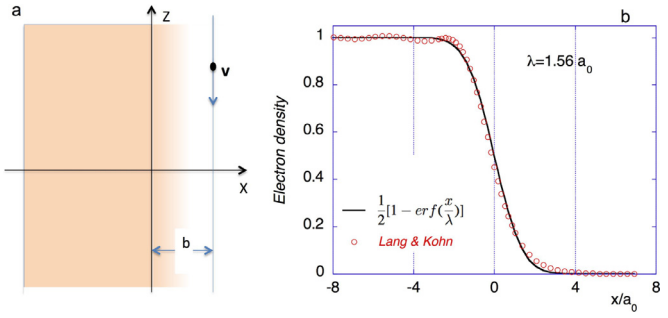

Fig. 1. (a) Sketch of the probe interacting with a diffuse interface. (b) Profile of the unperturbed charge density near the interface. Red circles (∘) correspond to the Table I ($r_s = 2a_0$) of Ref. [51], while the black line is the analytical approximation used in the present work. (For interpretation of the references to color in this figure legend, the reader is referred to the web version of this article.)

Eq. (7) is an integral equation, which in the case of a metal described by a Drude dielectric function is strictly equivalent to Poisson equation. In particular, it is straightforward to prove this last statement in the case of a homogeneous medium. For an arbitrarily shaped sharp interface Eq. (7) can be recast in terms of a surface density, leading to the same equation used in the *BEM* method [3]. In the case of a planar interface where the *local* plasmon frequency varies continuously along the normal direction x, [see Fig. 1a)], so that $\widetilde{\omega_p^2}(\mathbf{r}) = \widetilde{\omega_p^2}(x)$, Eq. (7) can be recast as a differential equation, which is also fully equivalent to the Poisson equation in a medium with a *local* Drude dielectric response $\epsilon(x, \omega) = 1 - \widetilde{\omega_p^2}(x)/[\omega(\omega + i\gamma)]$ [9].

Given that dispersive effects emerge in a simple way in the $\mathbf{k}$-space, we Fourier transform Eq. (7),

$$\omega(\omega + i\gamma)\rho(\mathbf{k}, \omega) - \frac{1}{2\pi}\int dq_x \frac{q_x k_x + Q^2}{q^2}\widetilde{\omega_p^2}(k_x - q_x)\rho(\mathbf{q}, \omega) = \frac{1}{2\pi}\int dq_x \frac{q_x k_x + Q^2}{q^2}\widetilde{\omega_p^2}(k_x - q_x)\rho_0(\mathbf{q}, \omega), \tag{8}$$

where $\mathbf{Q} \equiv (q_y, q_z)$ stands for the parallel components of the momentum $\mathbf{q} = (q_x, \mathbf{Q})$, $\mathbf{k} = (k_x, \mathbf{Q})$ and $\widetilde{\omega_p^2}(k_x)$ is the Fourier transform of $\widetilde{\omega_p^2}(x)$.

In order to introduce the dispersion we assume that its effects are also ruled by a *local* parameter $\widetilde{\beta^2}(x)$, and that they can be described through an extra force in Eq. (8). The linearized pressure term of the hydrodynamic theory [52] provides a hint about the form of this correction, but it is not enough to determine its expression. Here this term has been taken in such a way that in both limiting cases, the homogeneous medium and the sharp interface, the known results of the dielectric theory are recovered. Under these conditions the simplest generalization of Eq. (8) is

$$\omega(\omega + i\gamma)\rho(\mathbf{k}, \omega) - \frac{1}{2\pi}\int dq_x \frac{\mathbf{q}.\,\mathbf{k}}{q^2}\,[\widetilde{\omega_p^2}(k_x - q_x) + \widetilde{\beta^2}(k_x - q_x)q^2]\rho(\mathbf{q}, \omega) = \frac{1}{2\pi}\int dq_x \frac{\mathbf{q}.\,\mathbf{k}}{q^2}\,\widetilde{\omega_p^2}(k_x - q_x)\rho_0(\mathbf{q}, \omega). \tag{9}$$

Note that the solution of this equation trivially verifies

$$\rho(\mathbf{k}, \omega) = \rho(-\mathbf{k}, -\omega)^*, \tag{10}$$

where z^* stands for the complex conjugate of z, a condition that ensures that the induced charge density $\rho(\mathbf{r}, t)$ is a real function.

Eq. (9) is a *Fredholm integral equation of the second kind* [53], which states the linearity of the response of the medium in a general form: both the free and the induced densities are linearly related through the convolution with a boundary-dependent kernel.

In the case of a homogeneous medium, $[\widetilde{\omega_p^2}(x) = \omega_p^2, \widetilde{\beta^2}(x) = \beta^2]$, the solution of this equation,

$$\rho(\mathbf{k}, \omega) = \frac{\omega_p^2}{\omega(\omega + i\gamma) - \omega_p^2 - \beta^2 k^2}\rho_0(\mathbf{k}, \omega), \tag{11}$$

matches the one obtained in the dielectric formalism with the HDF.

Assuming the continuity of the function $\widetilde{\beta^2}(x)$, this equation can be written back in the x space as:

$$\begin{aligned}&\{\omega(\omega + i\gamma) - \widetilde{\omega_p^2}(x) - \widetilde{\beta^2}(x)Q^2\}\rho(x, Q, \omega)\\ &\quad - \frac{1}{2}\frac{d\widetilde{\omega_p^2}(x)}{dx}\int dx' sgn(x - x')e^{-Q|x-x'|}\rho(x', Q, \omega)\\ &\quad + \frac{\partial}{\partial x}\{\widetilde{\beta^2}(x)\frac{\partial}{\partial x}\rho(x, Q, \omega)\}\\ &= \widetilde{\omega_p^2}(x)\rho_0(x, Q, \omega) + \frac{1}{4\pi}\frac{d\widetilde{\omega_p^2}(x)}{dx}E_{0x}(x, Q, \omega),\end{aligned} \tag{12}$$

where *sgn*(x) stands for the sign function. Finally this equation can be fully recast in the real space as

$$\begin{aligned}&\widetilde{\beta}^2(\mathbf{r})\nabla^2\rho(\mathbf{r}, \omega) + [(\omega + i\gamma)\omega - \widetilde{\omega}_p^2(\mathbf{r})]\rho(\mathbf{r}, \omega)\\ &\quad + \frac{1}{4\pi}\nabla\widetilde{\omega}_p^2\,\nabla\int d\mathbf{r}'\frac{\rho(\mathbf{r}', \omega)}{|\mathbf{r}' - \mathbf{r}|} + \nabla\widetilde{\beta}^2\nabla\rho(\mathbf{r}, \omega)\\ &= \widetilde{\omega}_p^2(\mathbf{r})\rho_0(\mathbf{r}, \omega) - \frac{1}{4\pi}\nabla\widetilde{\omega}_p^2\,\nabla\int d\mathbf{r}'\frac{\rho_0(\mathbf{r}', \omega)}{|\mathbf{r}' - \mathbf{r}|},\end{aligned} \tag{13}$$

which manifestly exhibits the independence of the response on the coordinate system used in its derivation. Therefore it is reasonable to think that this equation is valid for arbitrary shaped interfaces.

Eqs. (12) and (13) are integro-differential equations, and in a general case they look as cumbersome to solve as their counterpart in k space. Nevertheless, an interesting application of these equations is that of a sharp interface, where, although both functions $\widetilde{\omega_p}^2$ and $\widetilde{\beta}^2$ are not continuous at the interface, can be considered as the limiting case of a extremely thin interface. Then, inside the medium, Eq. (13) turns out to be a Helmholtz equation, which for simple shaped targets admits an analytical solution in terms of the natural coordinates associated to the geometry of the surface. The interface terms in $\nabla\widetilde{\beta^2}$ and $\nabla\widetilde{\omega}_p^2$ just provide the requested boundary condition. This procedure will be developed in the next section, where Eq. (12) will be used to check this approach, by comparing its results to these obtained in the *SRM* approximation.

The induced charge density provides full information about the probe-target interaction. For the particular case of a probe moving parallel to the surface with velocity $\mathbf{v} = (0, 0, v)$ and impact parameter b, (Fig. 1a) where the probe charge density is $\rho_0(\mathbf{k}, \omega) = 2\pi e^{-ik_x b}\delta(\omega - k_z v)$, one can remove the explicit k_z dependence of the induced charge density by writing $\rho(\mathbf{k}, \omega) = \hat{\rho}(k_x, Q, \omega)\delta(\omega - k_z v)$ where $Q^2 = k_y^2 + (\omega/v)^2$. Then the induced potential is

$$\phi_{ind}(\mathbf{r}, \omega) = \frac{1}{2\pi^2 v}\int dk_x dk_y \frac{\hat{\rho}(k_x, Q, \omega)}{k^2}e^{i(k_x x + k_y y)}e^{i\frac{\omega z}{v}}. \tag{14}$$

Making use of Eq. (10) one can calculate the momentum transfer per unit path length,

$$\frac{\Delta p_x}{\Delta z} = -\frac{1}{v}\frac{\partial\phi_{ind}}{\partial x}|_{traj} = -\int_0^\infty d\omega\int_0^\infty dk_y\int_{-\infty}^\infty dk_x k_x\Sigma(k_x, k_y, \omega) \tag{15}$$

$$\frac{\Delta p_z}{\Delta z} = -\frac{1}{v}\frac{\partial\phi_{ind}}{\partial z}|_{traj} = -\int_0^\infty d\omega\int_0^\infty dk_y\int_{-\infty}^\infty dk_x \frac{\omega}{v}\Sigma(k_x, k_y, \omega), \tag{16}$$

where the derivatives of the induced potential are evaluated at the probe position $[\mathbf{r} = (b, 0, vt)]$,

$$\Sigma(k_x, k_y, \omega) = \frac{-1}{\pi^3 v^2}\mathcal{I}m\left[\frac{\rho(k_x, Q, \omega)e^{ik_x b}}{k^2}\right] \tag{17}$$

and $\mathcal{I}m[R]$ stands for the imaginary part of R. The set of Eqs. (15) and (16) states that the scattering of the probe is the sum of the

contributions of excitations of energy ω and momentum $(k_x, k_y, k_z = \omega v^{-1})$, with excitation probability (per unit length) given by the function $\Sigma(k_x, Q, \omega)$. From Eq. (16) the energy loss probability per unit length is obtained as:

$$\frac{dP(\omega)}{d\omega\ dz} = \int_0^\infty dk_y \int_{-\infty}^\infty dk_x\ \ \Sigma(k_x, k_y, \omega). \tag{18}$$

3. Analytical solution for a sharp interface

Let us consider a semi-infinite medium bounded by a flat interface at $x = 0$. The medium is confined in the left half-space, so that $\widetilde{\omega_p^2}(x) = \omega_p^2 H(-x)$ and $\widetilde{\beta^2}(x) = \beta^2 H(-x)$, where $H(x)$ is the Heaviside function and ω_p^2 and β^2 are the bulk values of these parameters in the medium.

3.1. External trajectory

When the probe moves outside the metal ($b > 0$) Eq. (12) admits a simple piecewise solution that only depends on an arbitrary function $A(Q, \omega)$:

$$\begin{aligned}\hat{\rho}(x, Q, \omega) &= A(Q, \omega)e^{\mu x} && x < 0\\ &= 0 && x > 0,\end{aligned} \tag{19}$$

where μ is the root of the equation $\mu^2 = Q^2 + \beta^{-2}[\omega_p^2 - \omega(\omega + i\gamma)]$ with positive real part. To calculate $A(Q, \omega)$, one can formally integrate Eq. (12) in an infinitesimal interval around $x = 0$. Then the surface terms of this equation lead to the following boundary condition at the interface:

$$\omega_p^2 \int_{-\infty}^0 dx e^{Qx}\hat{\rho}(x, Q, \omega) - 2\beta^2 \frac{\partial}{\partial x}\hat{\rho}(x, Q, \omega)|_{x=0^-} = 2\pi\omega_p^2 e^{-Qb}, \tag{20}$$

where the derivative of the charge density has been evaluated in the limit $x \to 0^-$. The coefficient $A(Q, \omega)$ can be straightforwardly obtained from Eq. (20), so that the induced charge density is

$$\begin{aligned}\hat{\rho}(x, Q, \omega) &= \frac{2\pi\omega_p^2(Q + \mu)e^{-Qb}}{\omega_p^2 - 2\beta^2\mu(Q + \mu)}e^{\mu x} && x < 0,\\ &= 0, && \\ x > 0.\end{aligned} \tag{21}$$

By writting this solution back in **k** space,

$$\hat{\rho}(k_x, Q, \omega) = \frac{2\pi i\omega_p^2(Q + \mu)e^{-Qb}}{\omega_p^2 - 2\beta^2\mu(Q + \mu)}\frac{1}{k_x + i\mu}, \tag{22}$$

we find that the k_x dependence of the induced density is not quadratic, reflecting the anisotropy of the medium response in the direction normal to the interface. In the limit of very weak dispersion ($\beta \to 0$) expression (22) reduces to

$$\hat{\rho}(k_x, Q, \omega) = \frac{2\pi\omega_p^2}{\omega_p^2 - 2\omega(\omega + i\gamma)}e^{-Qb}. \tag{23}$$

The independence of this expression on k_x implies that in the local approach the induced charge is on the surface. It can be easily shown that the corresponding surface charge density is the same obtained in the local dielectric approach for a Drude dielectric function [2].

Once the induced charge density is known, the induced potential outside the metal ($x > 0$) is easily calculated:

$$\phi_{ind}(\mathbf{r}, \omega) = \frac{\omega_p^2}{v}\int \frac{dk_y}{Q}\frac{e^{-Q(x+b)}e^{ik_y y}e^{i\frac{\omega z}{v}}}{[\omega_p^2 - 2\beta^2\mu(Q + \mu)]}. \tag{24}$$

The dispersion relation of the surface plasmon is then given by the poles of integral function, i.e., $2\beta^2\mu(Q + \mu) = \omega_p^2$. Neglecting the damping, and for small values of Q, the following dispersion relation is obtained:

$$\omega(Q) = \omega_s(1 + \frac{\beta Q}{2\omega_s}), \tag{25}$$

where $\omega_s = \omega_p/\sqrt{2}$ is the frequency of the undispersed surface plasmon. This dispersion relation is a well known expression, first derived by Ritchie using Bloch's equation [30], and by Ritchie and Marusak using the *SRM* [31]. Actually, following ref. [34] it is easy to prove that the induced potential (24) is the same as the one derived in the *SRM* for the HDF. This potential is also the solution of the hydrodynamic model used by García-Lekue and Pitarke [54].

The energy loss probability per unit length is calculated from Eq. (18). After integration on k_x, it reduces to the following expression:

$$\frac{dP}{dz\ d\omega} = \frac{2\omega_p^2}{\pi v^2}\int_0^\infty dk_y \frac{e^{-2Qb}}{Q} Im[\frac{1}{\omega_p^2 - 2\beta^2\mu(Q + \mu)}]. \tag{26}$$

This result also matches the one obtained with the *SRM* [34] or with the hydrodynamic model of ref. [54]. In the limit $\beta \to 0$, Eq. (26) reduces to the well known local expression [55].

3.2. Inner trajectories

When the probe is traveling parallel to the interface through the medium ($b < 0$), the regular solution of Eq. (12) can be splitted as:

$$\begin{aligned}\hat{\rho}(x, Q, \omega) &= A(Q, \omega)e^{-\mu|x-b|} + B(Q, \omega)e^{\mu x} && x < 0\\ &= 0 && x > 0,\end{aligned} \tag{27}$$

where μ is defined as in Eq. (19). The coefficients A and B can be calculated from the discontinuity of the derivative of $\rho(x, Q, \omega)$ at the probe position ($x = b$) and from the boundary condition (Eq. 20) at the interface. After some trivial algebra one finds they are given by:

$$\begin{aligned}A(Q, \omega) &= -\frac{\pi\omega_p^2}{\mu\beta^2}\\ B(Q, \omega) &= \frac{2\pi\omega_p^2(Q + \mu)e^{\mu b}}{\omega_p^2 - 2\beta^2\mu(Q + \mu)}\\ &+ \frac{2\pi\omega_p^2(Q + \mu)}{\omega_p^2 - 2\beta^2\mu(Q + \mu)}[\frac{\omega(\omega + i\gamma)e^{Qb}}{\omega_p^2 - \omega(\omega + i\gamma)} + \frac{\omega_p^2 e^{\mu b}}{2\beta^2\mu(Q - \mu)}].\end{aligned} \tag{28}$$

The physical meaning of Eq. (27) is more clear when written in the k space:

$$\hat{\rho}(k_x, Q, \omega) = \frac{2\pi\omega_p^2 e^{-ik_x b}}{\omega(\omega + i\gamma) - \omega_p^2 - \beta^2 k^2} + \frac{iA(Q, \omega)e^{\mu b}}{k_x - i\mu} + \frac{iB(Q, \omega)}{k_x + i\mu}. \tag{29}$$

The contribution of the first term of Eq. (29) to the momentum transfer (Eq. (15)–(17)) has no dependence on the impact parameter b; this term just represents the screening charge density due to bulk excitations in a unbounded medium (Eq. (11)). The energy loss derived from this term consists of the sum of contributions of bulk plasmons $\omega(k)$ with dispersion relation $\omega(k) = \sqrt{\omega_p^2 + \beta^2 k^2}$. The exponential dependence on b of the remaining two terms of Eq. (29) identifies them as the surface contribution to the induced charge density. The frequencies at which these contributions occur are centered at the poles of the coefficients A and B. The coefficient A presents a single pole at $\mu = 0$, which also corresponds to bulk plasmons, but now the dispersion only depends on the parallel momentum Q: $\omega(\mathbf{k}) = \sqrt{\omega_p^2 + \beta^2 Q^2}$, reflecting the anisotropy of the response introduced by the interface. The first term of B in Eq. (28) is the same found for external trajectories (Eq. (21)), and its pole ($\omega_p^2 - 2\beta^2\mu(Q + \mu) = 0$) represents excitations of surface plasmons with dispersion relation given by (25). The poles of the second term of B correspond to surface plasmon excitations as well as to bulk modes $\mu = 0$, and $\omega = \omega_p$). These surface corrections to the bulk plasmon excitation constitute the well known *Begrenzung* (or

Boundary) effect [1].

It can be demonstrated that the potential induced by the charge density (29) is also the same obtained in the *SRM* for the *HDF*.

Note that the piecewise solutions (21) and (27) are not strictly consistent with the initial Eq. (12), which implicitly requires the continuity of $\hat{\rho}(x, Q, \omega)$ along the interface. A simple inspection proves that the solution (22) does not satisfy exactly the Fredholm Eq. (9); it is just an approximate solution, suitable for small k_x values. The explanation of this apparently contradictory result is that the current theory implies a smooth variation of the density profile along the interface, and therefore the use of this model in sharp surfaces is not fully consistent. In Fig. 2 we compare the induced charge density obtained by solving numerically the Fredholm equation for a sharp interface (continuous red line) to that of the approximate solution (Eq. (22)) (dotted red line); the overall shape of these plots is rather similar near the k_x origin; the real part being an odd function, while the imaginary part is an even one. The difference of the imaginary part occurs for large k_x values ($k_x > 0.3$ Å^{-1}), with a negligible contribution to the stopping power. Actually an arguably better -but still approximate- solution of Eq. (12) could have been obtained by taking in Eq. (20) the average value of the derivative $\partial_x\widetilde{\beta}$ at both sides of the interface. As the main aim of this section is to show the soundness of the theoretical approach, we have not studied this solution. From now on, results derived from the approximate solutions (22) and (27) will be referred as *SRM*.

In the same way the response of a film can be straightforwardly calculated, recovering the results found by de Andres and coworkers [39].

The fact that the present model recovers the known results in two limiting cases; the unbounded medium (Eq. (11)), as well as that of a semi-infinite medium bounded by a sharp interface (Eqs. (22) and (29)) means that this model provides a solid approach to the study of nonlocal effects in more realistically modeled interfaces.

4. EELS In diffuse interfaces

The former formalism is now applied to the study of the excitations induced by a fast electron moving parallel to a diffuse Al-vacuum interface, where the unperturbed electron density $n(x)$ varies continuously along the interface as shown in Fig. 1 a). The density profile has been modeled by fitting the tabulated values of Ref. [51] for $r_s = 2a_0$ by a simple function, so that the *local* plasmon frequency writes

$$\widetilde{\omega_p^2}(x) = \frac{\omega_p^2}{2}[1 - erf(\frac{x}{\lambda})] \longrightarrow \widetilde{\omega_p^2}(k_x) = \omega_p^2[\pi\delta(k_x) + \frac{i}{k_x}e^{-\frac{1}{4}\lambda^2 k_x^2}], \tag{30}$$

where $erf(x)$ stands for the error function [56]. The best fit corresponds to $\lambda = 1.56a_0$. Although this parametrization irons out the Friedel oscillations present in the tabulated profile, the function (30) represents a reliable approximation to these data. In our calculation we have taken $\omega_p = 15.3$ eV ($r_s = 2.12\ a_0$) and $\gamma = 1$ eV.

One reasonable ansatz for the function $\widetilde{\beta^2}(x)$ is to assume the same spatial profile of $\widetilde{\omega_p^2}(x)$ (Eq. (30)); for such a sharp interface the result does not differ significantly from the *local* function extrapolated from the unbounded medium relation given by Eq. (2) and it greatly simplifies the computation. Then Eq. (9) writes as:

$$\begin{aligned}[\omega(\omega + i\gamma) - \frac{1}{2}(\omega_p^2 + \beta^2 k^2)]\hat{\rho}(k_x, Q, \omega) \\ + \frac{i}{2\pi}\mathbb{P}\int dq_x \frac{\mathbf{k}.\mathbf{q}}{q^2}[\omega_p^2 + \beta^2 q^2]\frac{e^{-\frac{\lambda^2}{4}(q_x - k_x)^2}}{q_x - k_x}\hat{\rho}(q_x, Q, \omega) \\ = 2\pi\widetilde{\omega_p^2}(b)e^{-ik_x b} + i\omega_p^2\int dq_x \frac{q_x e^{-iq_x b}}{q^2}e^{-\frac{\lambda^2}{4}(q_x - k_x)^2},\end{aligned} \tag{31}$$

where $\mathbb{P}$ stands for the Cauchy principal value of the integral.

A computational procedure to solve this equation is briefly discussed in Appendix A.

Fig. 2 shows the k_x dependence of the real and imaginary parts of the charge density, (at $\omega_s = \omega_p/\sqrt{2}$ and $k_y = 0$), induced by a 100 keV electron traveling with impact parameter $b = 1$ nm for different interface models. To visualize the combined effect of the density profile and dispersion three plots corresponding to the sharp interface have been added: *SRM* $\lambda = 0$ (Eq. (22)), *nonlocal* $\lambda = 0$ (Eq. (31)), and *local* $\lambda = 0$ (Eq. (23)), as well as the *local* $\lambda = 1.56a_0$, obtained from Eq. (31) with $\beta^2 = 0$. The close similarity of the two nonlocal plots for a sharp interface has been already discussed in the previous section. One remarkable feature of these plots is that all them take the same value at the k_x origin. Given that $\hat{\rho}(k_x = 0, Q, \omega) = \int dx\hat{\rho}(x, Q, \omega)$, i.e., the total charge induced along the direction normal to the interface, this coincidence just states that the total charge required to screen the external field inside the metal is roughly the same, irrespectively of the sharpness of the interface or of the **k** dependence of the response of the medium. The most relevant effect of the surface diffuseness in the scattering probability derives from the change of parity of the imaginary part around $k_x = 0$: the three plots corresponding to the sharp interface behave locally as even functions, while those corresponding to the diffuse interface have a non-negligible slope. This fact is relevant given that at the surface plasmon resonance the real part of the charge density is negligible, and therefore it is its imaginary part the one that defines the scattering function $\Sigma(k_x, k_y, \omega)$.

In Fig. 3 a) it is shown the **k** contribution to the loss probability per unit length, i.e.; the function $v\Sigma(k_x, k_y, \omega)$ at the surface plasmon energy ω_s, for a 100 keV electron with impact parameter $b = 1nm$. It represents

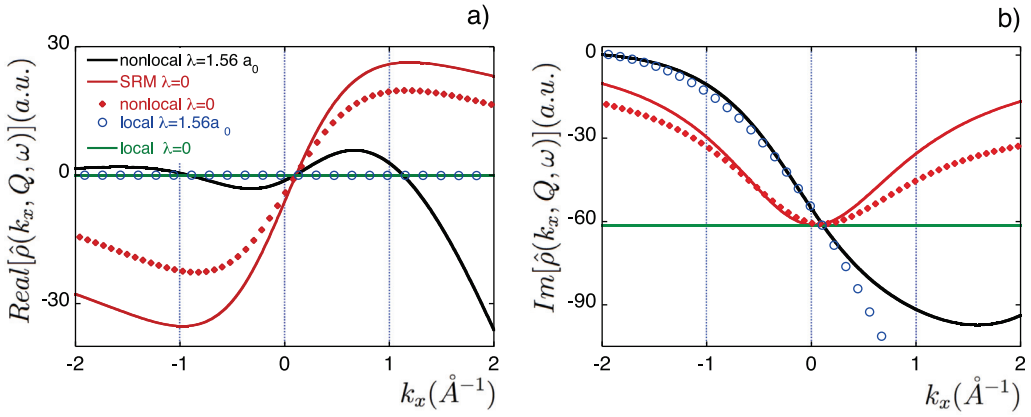

Fig. 2. Real and imaginary parts of the induced charge density $\hat{\rho}(k_x, Q, \omega)$ at $\omega_s = \omega_p/\sqrt{2}$ and $k_y = 0$. The probe energy is 100 keV ($v = 76$ a.u.) and the impact parameter $b = 1$ nm. Plots corresponding to different models of the interface, *local/nonlocal*, diffuse ($\lambda = 1.56a_0$) / sharp ($\lambda = 0$) are labelled as shown in *a*). Parameters of the metal response: $\hbar\omega_p = 15.3$ eV, $\hbar\gamma = 1$ eV and $\beta^2 = 0.49$ a.u.

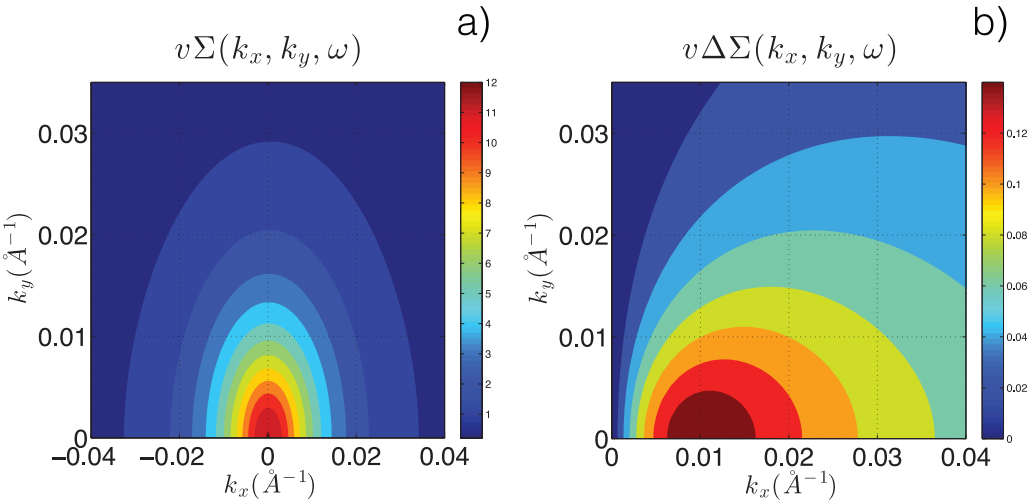

Fig. 3. a) Momentum contribution to the loss peak at ω_s. b) Transverse anisotropy of the loss function: $\Delta\Sigma(k_x, k_y, \omega) = \Sigma(k_x, k_y, \omega) - \Sigma(-k_x, ky, \omega)$. Parameters of the simulation as in Fig. (2).

the probability of collecting an electron scattered at ω_s with momentum $(k_x, k_y, \Delta k_z = \omega_s v^{-1})$. Here we see that most of the electrons are scattered with very low momentum transfer, so that for standard STEM acceptance angles almost all the scattered electrons are collected in the detector. In Fig. 3b) we display the difference of the probability of exciting plasmons with $-k_x$ and k_x transverse momentum. This anisotropy is a direct consequence of the diffuseness of the interface; neglecting the damping, in sharp interfaces (Eqs. (22) and (23)), $\Sigma(-k_x, k_y, \omega) = \Sigma(k_x, k_y, \omega)^{\star}$, and consequently the contribution to the transverse momentum transfer, Δp_x, arises from the real part of the induced density, whereas the longitudinal component Δp_z arises from its imaginary part. In particular around ω_s, where the real part of the induced density is very small, the contribution to the transverse momentum is negligible. The fact that for a sharp interface $\Delta p_x \sim 0$ is a physical consequence of sharpness of the interface; in the local case the induce charge density lies on the interface, so that actually there is not transverse momentum transfer associated to the surface excitations, whereas the specular reflection assumed in the nonlocal approach makes both $\pm k_x$ excitations rougly equiprobable. Although the k_x anisotropy shown in Fig. 3b) is hardly resolvable with the current STEM set-up, this effect could be relevant to understand the anomalous momentum transfer reported by Batson and coworkers [26]. Note that although the positive correction shown in Fig. 3b) tends to reinforce the attractive character of the transverse force at ω_s, this contribution is relevant in the overall excitation range, so that the contribution of the full $\omega - k_y$ space, as well as its impact parameter dependence, should be more carefully studied.

In Fig. 4 we study the effect of the density spill-out on the loss spectrum by comparing the loss probability per unit length experienced by an electron moving near an Al diffuse interface to the *SRM* result. In the case of external trajectories, spectra corresponding to the local dielectric approaches are also plotted; sharp (*local* $\lambda = 0$) and diffuse interface (*local* $\lambda = 1.56a_0$). For distant probe trajectories (Fig. 4a) the loss spectra are rather similar; this fact is a consequence of the similarity of the induced density in the reduced $\mathbf{k}$ interval contributing to the inelastic scattering (Fig. 2). For beam trajectories closer to the surface [Fig. 4 b)] however, the energy of loss peak presents a larger dispersion, and the intensity of the *local* $\lambda = 0$ plot is significantly higher, a consequence of the unphysical extension of the dielectric response to high k values. In Fig. 4b) the spectra have been extended above the bulk plasmon energy, confirming that probes with external trajectories are not able to excite bulk plasmons, even when traveling at grazing incidence. A recent theoretical work in the frame of the hydrodynamic model [43] has shown that bulk modes can be excited in nanoparticles by external probes. Preliminary results for nanoparticles obtained from Eq. (13) also confirm this last observation. The fact that in planar interfaces bulk modes are not present in the spectra suggests that the excitation of bulk modes by external probes is restricted to the case of small targets where the charge density penetration depth around ω_p is comparable to the size of the target.

For trajectories inside the metal (Fig. 4c) and d)) the spectra feature the *Begrenzung effect* found in Section 3: for probe positions very close to the interface (Fig. 4c)) the spectra consist basically of a large surface peak around 11 eV; the bulk plasmon excitation is almost completely inhibited in the sharp interface, whereas the diffuse interface plot shows a small shoulder around the bulk plasmon energy ω_p. Note that the total integrated probability is roughly the same in both models, suggesting that the probability fulfills a Bethe-like sum rule [57]. In the case of a beam well inside the metal (Fig. 4d) the loss spectra feature both bulk and surface peaks. Comparison with the loss spectrum in an unbounded medium (dotted blue line in Fig. 4d) indicates that in addition to the reduction of the bulk loss peak intensity, it is now blue shifted with respect to the energy corresponding to the unbounded case ($\omega = 15.35$ eV) to the values 15.40 eV (present theory) and 15.57 eV (*SRM*). This surface induced dispersion of the bulk plasmon reflects the different contribution of high k_x components of the induced charge density: in a sharp interface the fact that the induced density should vanish at the interface poses a constraint on the possible values of k_x; the allowed momenta should be of the form: $k_x = \pi n b^{-1}$, n being an odd integer. For small values of b this quantification severely cancels the low k_x contributions to the loss spectrum; so that on the one hand it implies a lowering of the intensity of the plasmon peak, and on the other hand the energy of the allowed excitations, $\omega_p(\mathbf{k}) = \omega_p + \beta^2\mathbf{k}^2$, is then larger than that corresponding to an unbounded medium. The effect of the electron spill-out in the bulk excitation probability is twofold; on the one hand the shift of the bulk peak is marginally smaller, and on the other hand near the interface (Fig. 4 c)) the inhibition of the bulk excitations is not total. Both effects are most likely to be a consequence of the fact that in this case the former k_x quantification condition is to some extent relaxed and the cancelation of the low k_x components is not total.

A remarkable feature of these plots is the close resemblance of the spectra corresponding to $b = \pm .1nm$, a result which reflects the continuity of the induced potential as a function of b along the interface.

In Fig. 5 we study the combined effects of the dispersion and the spill-out in the characteristic features of the loss spectra for non-penetrating trajectories as a function of the impact parameter. In Fig. 5a) the impact parameter dependence of the peak intensity is analyzed. At large

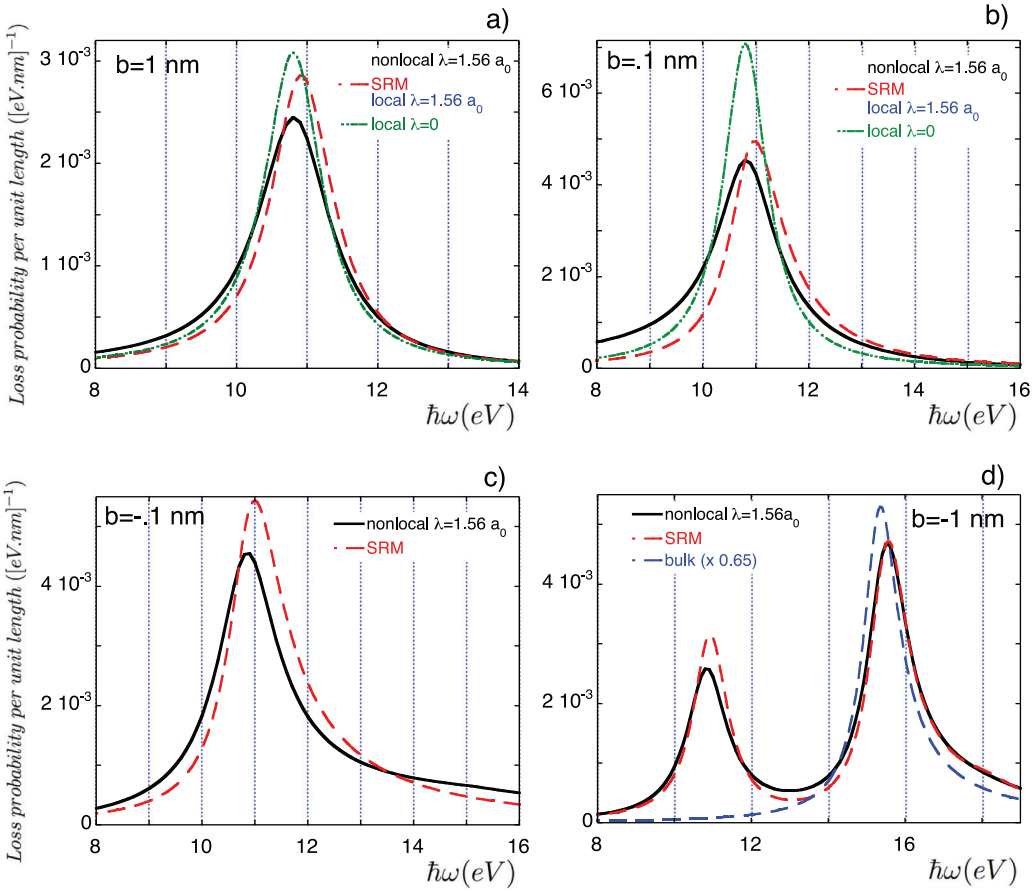

Fig. 4. EEL spectra for a 100 keV electron traveling parallel to an Al interface, for four different impact parameters: $b = 1$ nm (a), $b = 0.1$ nm (b), $b = -0.1$ nm (c) and $b = -1$ nm (d). Solid black lines (labeled as *nonlocal* $\lambda = 1.56\ a_0$) correspond to the current theory. The *SRM* spectra (as well those of the local theory for diffuse ($\lambda = 1.56\ a_0$) and sharp ($\lambda = 0$) interfaces for external probe trajectories) have been added for comparison. In (d) the dash-dotted blue plot corresponds to the case of an unbounded medium with the HDF (Eq. (1)). Parameters of the interface as in Fig. (2). (For interpretation of the references to colour in this figure legend, the reader is referred to the web version of this article.)

impact parameters all the models lead to a similar plasmon excitation probability. It is an obvious consequence of the smallness of the momentum values of the components involved in the scattering, a fact that, on the one hand, makes negligible dispersive corrections and that, on the other hand, given that their large wave length is much larger than the interfacial thickness ($\sim \lambda$) entails that these components are insensitive to the interface profile. At grazing incidence, laying aside the local theory for a sharp interface, which presents a logarithmic divergence as $b \to 0$, it is mainly the interface profile, λ, what determines the impact parameter dependence of the loss peak intensity; diffuse profile plots are almost overlapping functions, as well as those corresponding to the sharp dispersive interface. The inset of this figure shows that this agreement between the plots corresponding to the diffuse interface occurs even for beam trajectories well inside the tail of the charge profile.

In Fig. 5b), we analyze the impact parameter dependence of the loss peak energy. The plot corresponding to the local approach in a diffuse interface (blue circles) shows that the effect of the spill-out is just to reduce the surface excitation energy; this red-shift becomes more relevant as the beam is closer to (and outside) the interface. The brisk increase of the energy near the interface occurs for beam trajectories very close to the interface ($b \leq \lambda \sim 0.1$nm), i.e., when the probe is actually passing through a dilute electron gas. Both nonlocal spectra corresponding to sharp interfaces exhibit a significant blue-shift relative to ω_s, a consequence of the surface plasmon dispersion which is larger for the *SRM*. The plot corresponding to the non sharp dispersive interface (*nonlocal* $\lambda = 1.56 a_0$) shows that the effect of the spill-out compensates to a large extent the blue shift induced by the dispersion. The shift is noticeable only at grazing incidence, when the probe travels through the tail of the unperturbed gas density. The smallness of this correction ($\Delta\omega \sim 9$ meV at $b = 1$ nm) confirms the suitability of the local dielectric approach for primary spectroscopy. The thickness of the interface λ proves to be critical to determine the energy of the interface plasmon; so for instance, for $\lambda = 2a_0$ the plot $\omega(b)$ turns out to be very flat, lying about 2 meV below the local one (*local* $\lambda = 0$).

These plots are directly connected with the surface plasmon dispersion relation; the field created by the probe at the interface goes as $e^{-Q|b|}$, so that $|b|^{-1}$ poses an effective cutoff to the range of Q components contributing to the loss spectrum. For a sharp interface the local theory (continuous green line) predicts no b dependence of the surface plasmon energy (poles of $\hat{\rho}(k_x, Q, \omega)$ in Eq. (23)), thereby its plot is quite flat; the small variation of the loss peak energy in this figure (about 12 meV along the full range of the plot) derives from the damping of the dielectric function. For diffuse interfaces Feibelman found that the local theory predicted negative dispersion of the surface plasmon: $\omega_s(Q) = \omega_s(0)[1 - \frac{1}{2}QReal(d_\perp)]$, where $d_\perp$ is the centroid of the induced density [8]. The corresponding plot (*local* $\lambda = 1.56 a_0$) in Fig. 5 b) shows a qualitative agreement with this result. In the dispersive diffuse interface the almost flat plot suggests a weak positive dispersion relation of the interface plasmon. This result is in reasonable quantitative agreement with the surface plasmon dispersion relation calculated by Ahlqvist and Apell, $\omega_s(Q) = \omega_s(0)(1 + \frac{1}{2}\Gamma Q)$, where $\Gamma = 0.08$ Å for the Lang-Kohn profile [48]. For $Q_{\min} \sim \omega v^{-1}$ it leads to a shift of about 4 meV, a value close to the one found in the

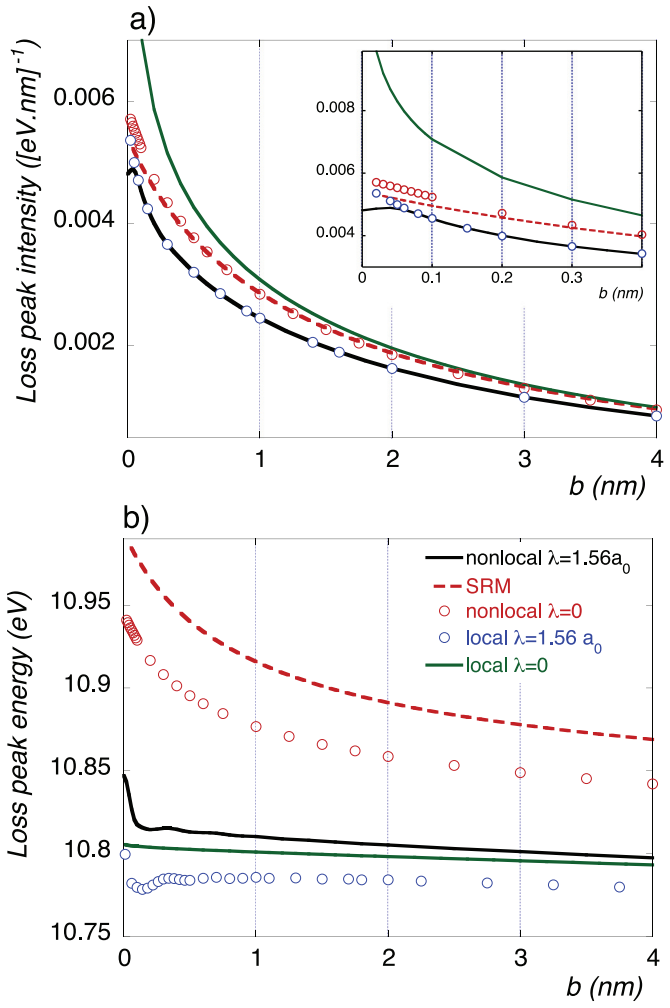

Fig. 5. Intensity (a) and energy (b) of the loss peak as a function of the impact parameter b for an *Al*-vacuum interface. Both nonlocal plots (labeled as *nonlocal* $\lambda = 1.56a_0$ and *nonlocal* $\lambda = 0$), as well the *local* $\lambda = 1.56a_0$ have been calculated from Eq. (31). The SRM plot and the one labeled as *local* $\lambda = 0$ from Eq. (26) and reference [55] respectively. The inset in (a) shows the detail of the plots for small values of b. Plot colour code as shown in Fig. b). Electron energy $E = 100$ keV and the parameters of the metal as in Fig. (2).

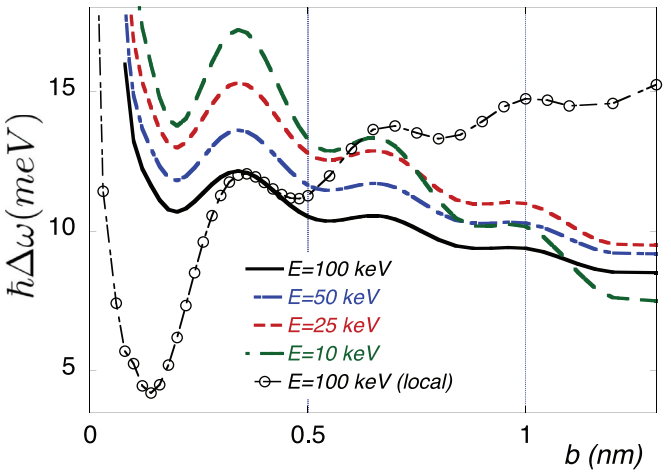

Fig. 6. Shift of the energy of the loss peak as a function of the impact parameter b for four energies of the probe. The the local plot (◦) has been shifted upwards by 30 meV to fit in the figure (see Fig. 5b). In all the plots $\lambda = 1.56a_0$.

corresponding plot of Fig. 5 b) at large impact parameters. This positive weak dispersion could also be inferred from Ref. [45] for an interface of similar thickness.

Although negative slopes in the surface plasmon dispersion have been experimentally observed in simple metals [58–61], the dispersion relation of the Al surface plasmon has been a matter of controversy over the years. Although inelastic low energy electron diffraction experiments by Duke and coworkers [62], indicated a negative slope of the plot $\omega_s(Q)$ at $Q = 0$, this result was not confirmed by *EELS* experiments [63,64]. More recently angle-resolved energy loss experiments of slow electrons (50 eV) in Al reported by Chiarello and coworkers confirmed the negative slope of the dispersion relation [65]. Note that usually the term of *Surface Plasmon Dispersion* assumes that the plasmon frequency depends just on the parallel momentum; i.e., $\omega(Q)$, neglecting the dependence of the excitation energy on the normal component. This assumption is consistent with the *SRM* where the loss probability can be written as an integral on Q (Eq. (26)), but it is not suitable in a more general case. In Fig. 6 we study the dependence of the dispersion of the loss peak energy on the impact parameter for different probe velocities. In order to remove the influence of the damping, the shifts have been calculated relative to the plasmon energy calculated in the local approach to the sharp interface [55]. Away from the interface ($b \gtrsim 4\lambda$) the plots can be described as a linear base line with negative slope plus some weak oscillatory corrections. The slope of the base lines roughly scale as v^{-1}, suggesting that for distant trajectories (or small values of Q) the dispersion presents the expected linear dependence on $Q \sim \omega v^{-1}$, i.e., a positive dispersion relation $\omega_s(Q)$. Nevertheless, for closer -but still outside the density tail- trajectories, $\lambda \lesssim b \lesssim 4\lambda$ all the plots exhibit a marked red-shift suggesting that the of large $\mathbf{k}$ contribution presents a noticeable negative dispersion.

The range of $\mathbf{k}$ involved in the Chiarello's experiment is at least an order of magnitude larger than the one probed in STEM, so both techniques actually probe different regions of the excitation spectrum. The results displayed in Figs. 5b and 6, shows that for *Al* the dispersion relation is quite flat in the low k range involved in the inelastic scattering of fast electrons, and that it critically depends on the parameter λ. Nevertheless, the negative change in the slope shown in these plots at grazing incidence implies that the contribution of large k components tends to lower the excitation energy, reflecting a negative dispersion in a momentum region out of the significant Q range involved in STEM experiments. Note that also the small differences in the response along different crystallographic directions could be responsible for the dispersion of the experimental data, as suggested by Krane and Raether [64].

In Figs. 5b and 6 the loss peak energy presents a weak enhancement at some equispaced values of b. The position of these oscillations does not depend on the probe velocity, i.e., on Q, therefore they are associated to transverse excitations, an assumption supported by their equispaced positions and by the fact that these excitations are also present at the same position in the local plot. They likely correspond to the so-called *Multipole Surface Plasmons* [45], which have been experimentally observed in reflexion experiments with low energy electrons [65]. These small structures in the $\omega(b)$ plot can hardly be detected by *EELS* experiments; in addition to the required meV resolution, these excitations occur at large k_x values, and therefore the scattered electrons would be out of the collector aperture, but they could be relevant in order to correctly estimate the transverse momentum transfer at small impact parameters.

5. Conclusions

We have presented a new nonretarded approach to the nonlocal interaction between a fast electron-probe and a metallic interface whose unperturbed charge density varies smoothly in the normal direction. The response of the medium is given by the induced charge density, which in its turn is calculated in terms of the parameters of a

nonlocal bulk dielectric function containing the information about the interface profile. In this way one avoids the problems posed by the standard (*SRM*) application of the nonlocal dielectric theory.

This theory has been applied to a realistically shaped Al-vacuum interface, finding that the effect of the density profile compensates to a high extent the blue shift of the loss peak energy predicted by *SRM*, in good agreement with previous theoretical and experimental results. The balance between nonlocal and spill-out effects implies that the energy of interface excitations is well given by the local approach for sharp interfaces. The dispersion relation of the interface excitations also provides a reasonable explanation to the spread of the experimental results.

The results reinforce the idea that a sound dispersive approach to interface excitations in *EELS* requires account to be taken of the density profile along the interface, because the high momentum components required to model the induced charge density in sharp interfaces lead to a severe overestimation of the blue shift of the loss peak.

We have also shown that in the case of diffuse interfaces there is a non-negligible transverse momentum transfer associated to the interface plasmon excitation.

We have presented a generalization of this theory to study plasmon excitations in targets of simple geometry, susceptible to be described by separable coordinates (films, spheres, cylinders, dimmers etc). In particular it allows the study of the size effects in the plasmon excitation in nanoparticles, where nonlocality introduces a new and relevant length scale.

As presented in this paper, the main limitation of the theory is that it is only applicable to simple metal-vacuum interface, where the medium response can be expressed by a couple of *local* parameters: $\widetilde{\omega_p^2}$ and $\widetilde{\beta^2}$. The extension of this approach to an interface between two free electron metals, as the one studied in ref. [9], is trivial; it just requires the change in the profile density (Eq. (30)). This theory can also be extended to deal with interfaces involving transition metals or insulators, described by bulk nonlocal Drude-Lorentz dielectric functions, as reported by Werner and coworkers [66]. In this case the medium would be modeled as a set of n different electron *bands*, each of them characterized by its unperturbed density $\omega_{p(k)}^2$, the dispersive parameter $\beta_{(k)}^2$ and the frequency of a binding oscillator $\omega_{0(k)}$ (here the index k labels diferent *bands*), and the response of the medium would be given by a set of n coupled Fredholm equations (one for each *band*). In this way this approach would allow to extract detailed information on the *local* composition of the sample from the interface plasmon maps.

A retarded formulation of this model is not straightforward, because then the response of the medium involves a vector field, the current, defined in the bulk. The extension of the retarded boundary element method to take into account the spatial dispersion of the response in abrupt interfaces proposed by Trügler and coworkers [44] could be of guidance for the retarded generalization of the current theory.

Acknowledgment

The author would like to thank A. Howie, P. M. Echenique, N. Zabala and P. Apell for many stimulating discussions. Financial support through Projects no. FIS2016-80174-P of Spanish MINECO and Consolidated Groups at UPV/EHU (grant no. IT1164-19) of the Basque Government is acknowledged.

Appendix A. Computing the induced charge density

The simplest method of solving a Fredholm equation of the second order is to consider a numerical integration rule (see for instance Ref. [67]). Let us consider the equation

$$g(x) = \int_a^b K(x, y) f(y) dy \tag{A.1}$$

where the function $g(x)$ and the integral kernel $K(x, y)$ are known and $f(y)$ is the unknown function. One can approximate this equation by a linear system of algebraic equations:

$$g(x_i) = \sum_{k=1}^{N} w_k K(x_i, y_k) f(y_k) \qquad a \le y_k \le b, \tag{A.2}$$

where $i, k = 1, 2, \ldots N$ and the points y_k and their corresponding weighting factors, w_k, are given by the particular integration method used. Then the values of the function $f(y)$ at the N points of the grid can be calculated, just by solving the linear system (A.2).

The contribution of the singularity to the principal part of the integral in Eq. (31) is accurately calculated from the odd derivatives of the integral function, which can be obtained by a simple interpolation of the function.

The accuracy of this method depends on two computational parameters; one is the cut-off Q_x posed to the q_x integration interval in Eq. (31), the other being the number N of points in the grid. In this work we have taken $N = 1999$ and $Q_x = 3a_0^{-1}$, a value which assures that the contribution of higher momenta to Eq. (31) is strongly damped by the gaussian factor associated to the interface thickness.

The simplest check of this numerical procedure is provided by the analytical result for a sharp interface metal-vacuum in the local approach [55], a result which should be recovered as the solution of Eq. (31) for $\lambda = 0$, $\beta^2 = 0$. Note that this case is also the most unfavorable one, because the cut-off associated to λ in the integral is missing. For the values of these parameters used in this work the error in the plot of the energy (Fig. 5b)) is smaller than 4 meV for $b \ge 1$ nm, reaching 6 meV at $b = 0.1$ nm, while the relative error in the loss peak intensity (Fig. 5a)) is below 6% in the full b range. The accuracy of this calculation is improved by extending Q_x; so for instance for $Q_x = 5a_0^{-1}$, these figures are reduced by half.

This procedure works much better for diffuse interfaces, where the gaussian factor in the integral of Eq. (31) assures a fast convergence of the solution of the Fredholm equation. In this case, the errors in Fig. 5 have been estimated by comparing the solution to that corresponding to $N = 999$ and $Q_x = 2a_0^{-1}$; then the error in energy peak is less than 2 meV, while the error of its height is about 1% in the full b range investigated in this work.

Supplementary material

Supplementary material associated with this article can be found, in the online version, at 10.1016/j.ultramic.2019.112835

References

[1] R.H. Ritchie, Phys. Rev. 106 (1957) 874–881.
[2] A. Rivacoba, N. Zabala, J. J. Aizpurua, Prog. Surf. Sci. 65 (2000) 1–64.
[3] F.J.G. de Abajo, J. Aizpurua, Phys. Rev. B. 56 (1997) 15873–15884.
[4] L.D. Marks, Solid State Commun. 43 (1982) 727–729.
[5] J.M. Cowley, Surf. Sci. 114 (1982) 587–606.
[6] A. Howie, R.H. Milne, J. Microsc. 136 (1984) 279–285.
[7] J. Aizpurua, A. Howie, F.J.G. de Abajo, Phys. Rev. B. 60 (1999) 11149–11162.
[8] P.J. Feibelman, Prog. Surf. Sci. 12 (1982) 287–407.
[9] A. Howie, F.J.G. de Abajo, A. Rivacoba, J. Phys C 20 (2008) 304205.
[10] R.G. Molina, A. Gras-Martí, A. Howie, R.H. Ritchie, J. Phys. C 18 (1985). 5335-45
[11] P. Moreau, N. Brun, C.A. Walsh, C. Collieux, A. Howie, Phys. Rev. B. 56 (1997) 6774–6781.
[12] A. Rivacoba, N. Zabala, New J. Phys. 16 (2014) 73048.
[13] N. Zabala, A. Rivacoba, Nucl. Instrum. Methods B 354 (2015) 105–108.
[14] C.A. Walsh, Philos. Mag. A 59 (1989) 227.
[15] N. Zabala, A. Rivacoba, P.M. Echenique, Surf. Sci. 209 (1989) 465–480.
[16] F.J.G. de Abajo, A. Howie, Phys. Rev. Lett. 80 (1998) 5180–5183.
[17] I. Romero, J. Aizpurua, G.W. Bryant, F.J.G. de Abajo, Opt. Express 14 (2006) 9988.
[18] A. Reyes-Coronado, R.G. Barrera, P.E. Batson, P.M. Echenique, A. Rivacoba, J. Aizpurua, Phys. Rev. B 82 (2010) 235429.
[19] A.A. Govyadinov, A. Konečná, A. Chuvilin, S. Vélez, I. Dolado, A.Y. Nikitin, S. Lopatin, F. Casanova, L.E. Hueso, J. Aizpurua, R. Hillenbrand, Nat. Commun. 8 (2017) 95.
[20] N. Talebi, W. Sigle, R. Vogelgesang, M. Esmann, S.F. Becker, C. Lienau, P.A. van Aken, ACS Nano 9 (2015) 77641.
[21] F.J.G. de Abajo, A. Howie, Phys. Rev. B. 65 (2002) 115418.
[22] D. Pines, D. Bohm, Phys. Rev. 85 (1952) 338–353.
[23] H. Watanabe, J. Phys. Soc. Jpn. 11 (1956) 112.
[24] P.E. Batson, J. Silcox, Phys. Rev. B 27 (1983) 5224–5239.
[25] J. Sprösser-Prou, A.v. Felde, J. Fink, Phys. Rev. B 27 (1983) 5799–5801.
[26] P.E. Batson, A. Reyes-Coronado, R.G. Barrera, A. Rivacoba, P.M. Echenique, J. Aizpurua, Nano Lett. 11 (2011) 3388–3393.
[27] J. Lindhard, K. Dansk, V. Selskab, Mat. Fys. Medd. 28 (8) (1954).
[28] N.D. Mermin, Phys. Rev. B 1 (1970) 2362–2363.
[29] D. Pines, P. Nozieres, The Theory of the Quantum Liquids, Benjamin, New York, 1966.
[30] R.H. Ritchie, Progr. Theor. Phys. 29 (1963) 607–609.
[31] R.H. Ritchie, A.L. Marusak, Surf. Sci. 4 (1966) 234–240.
[32] D. Wagner, Z. Naturforsch, Teil A 21 (1966) 634–642.
[33] R. Núñez, P.M. Echenique, R.H. Ritchie, J. Phys. C 13 (1980) 4229–4246.
[34] N. Zabala, P.M. Echenique, Ultramicroscopy 32 (1990) 327–335.
[35] B.B. Dasgupta, R. Fuschs, Phys. Rev. B 24 (1981) 554–561.
[36] R. Fuschs, F. Claro, Phys. Rev. B 35 (1987) 3722–3727.
[37] F.J.G. de Abajo, J. Phys. Chem. C 112 (2008) 17983–17987.
[38] J. Aizpurua, A. Rivacoba, Phys. Rev. B 78 (2008) 35404.
[39] P.L. de Andres, P.M. Echenique, D. Niesner, T. Fauster, A. Rivacoba, New J. Phys. 16 (2014) 23012.
[40] P.J. Feibelman, Phys. Rev. B 3 (1971) 220–222.
[41] J.M. McMahon, S.K. Gray, G.C. Schatz, Phys. Rev. Lett. 103 (2009) 97403. Phys. Rev. B **82** (2010)
[42] C. David, F.J.G. de Abajo, J. Phys. Chem. C 115 (2011) 19470–19475.
[43] T. Christensen, W. Yan, S. Raza, A.-P. Jauho, N.A. Mortensen, M. Wubs, ACS Nano 8 (2014) 1745–1758.
[44] A. Trügler, U. Hohenester, F.J.G. de Abajo, Int. J. Mod. Phys. B 31 (2017) 1740007.
[45] A.J. Bennett, Phys. Rev. B 1 (1970) 203–207.
[46] A. Eguiluz, S.C. Ying, J.J. Quin, Phys. Rev. B 11 (1975) 2118–2121.
[47] A. Eguiluz, J.J. Quin, Phys. Rev. B 14 (1976) 1347–1361.
[48] P. Ahlqvist, P. Apell, Physica Scripta 25 (1982) 587–591.
[49] O.K. Harsh, B.K. Agarwal, Phys. Rev. B 39 (1989) 8150–8152.
[50] P.E. Batson, Ultramicroscopy 9 (1982) 277–282.
[51] N.D. Lang, W. Kohn, Phys. Rev. B 1 (1970) 4555–4568.
[52] A.D. Boardman, Electromagnetic Surface Modes, Wiley, Chichester, UK, 1982.
[53] K.E. Atkinson, The Numerical Solution of Integral Equations of the Second Kind, Cambridge, Cambridge, 1997.
[54] A. García-Lekue, J.M. Pitarke, Phys. Rev. B 64 (2001) 35423.
[55] A. Howie, Ultramicroscopy 11 (1983) 141–146.
[56] M. Abramowitz, I.A. Stegun, Handbook of Mathematical Functions, Dover, New York, 1964.
[57] R.F. Egerton, Electron Energy-Loss Spectroscopy in the Electron Microscope, Plenum, New York, 1996.
[58] C. Kunz, Z. Phys. 196 (1966) 311–331.
[59] K.-D. Tsuei, E.W. Plummer, P.J. Feibelmann, Phys. Rev. Lett. 63 (1989) 2256–2259.
[60] K.-D. Tsuei, E.W. Plummer, A. Liebsch, K. Kempa, P. Bakshi, Phys. Rev. Lett. 64 (1990) 44–47.
[61] P.T. Sprunger, G.M. Watson, W. Plummer, Surf. Sci. 269/270 (1992) 551–555.
[62] C.B. Duke, L. Pietronero, J.O. Porteus, J.F. Wendelken, Phys. Rev. B 12 (1975) 4059–4070.
[63] T. Kloos, H. Raether, Phys. Lett. A 44 (1973) 157–158.
[64] K.J. Krane, H. Raether, Phys. Rev. Lett. 37 (1976). 1355-57
[65] G. Chiarello, V. Formoso, A. Santaniello, E. Colavita, L. Papagno, Phys. Rev. B. 62 (2000) 12676–12679.
[66] W.S.M. Werner, K. Glantschnig, C. Ambrosch-Draxl, J. Phys. Chem. Ref. Data 38 (2009) 1013–1092.
[67] W.H. Press, S.A. Teukolsky, W.T. Vetterling, B.P. Flannery, Numerical Recipes, Cambridge, New York, 1992.